Bulletin of Geophysics and Oceanography
Vol. 66, n. 4, pp. 477-494; December 2025
DOI 10.4430/bgo00505

Virtual sea surface temperature stations for the Turkish coastal gaps: a machine learning-driven fusion of satellite and *in-situ* data

M.H. Erkoç, C.N. Zengin and H.Ç. Çiçek

Department of Geomatic Engineering, Yildiz Technical University, Esenler-Istanbul, Turkey

(Received: 15 June 2025; accepted: 9 October 2025; published online: 19 December 2025)

ABSTRACT Accurate monitoring of sea surface temperature (*SST*) is vital for understanding regional climate variability, marine ecosystem dynamics, and long-term climate change. In this study, the consistency between satellite-derived *SST* data from the Copernicus Marine Environment Monitoring Service (CMEMS) and *in-situ* observations from 21 coastal stations operated by the Turkish State Meteorological Service was evaluated across the Turkish coastline. Initial assessments were based on classical statistical comparisons using the root-mean-square deviation and Pearson correlation. Subsequently, four machine learning (ML) regression models, linear regression, support vector regression, gradient boosting, and artificial neural networks, were applied to assess the predictive capability of CMEMS data for estimating *in-situ SST*. Among the models, GB achieved the best overall performance (coefficient of determination = 0.97, root-mean-square error = 0.84 °C), owing to its ability to effectively capture complex nonlinear relationships between datasets. Based on these results, a spatial gap analysis was conducted, and eight statistically optimised proxy observation points (termed virtual *SST* stations) were proposed to enhance *SST* coverage in underserved coastal segments. This study demonstrates a scalable (regionally adaptable) and objective methodology for optimising *SST* monitoring networks by integrating ML with geospatial analysis. The proposed approach offers practical benefits in enhancing climate resilience, improving *SST* anomaly forecasting, and supporting evidence-based marine resource management, such as fishery zoning or coastal ecosystem protection.

Key words: sea surface temperature, machine learning, Turkish seas, virtual observation stations, data integration, coastal monitoring optimisation.

1. Introduction

Sea surface temperature (*SST*) is a crucial parameter in oceanography, as it plays a pivotal role in influencing climate patterns, marine ecosystems, and regional environmental monitoring. *SST* affects atmospheric conditions through heat and moisture exchanges, thereby impacting weather phenomena and climate variability on both global and regional scales (Friedland and Hare, 2007; Pisano *et al.*, 2020; Yang *et al.*, 2021). Moreover, *SST* serves as a vital indicator of climate change, enabling scientists to identify long-term trends and assess their effects on oceanic systems (Bell and Goring, 1998; Chapanov *et al.*, 2017; Pisano *et al.*, 2020). Changes in *SST* are closely linked to shifts in marine biodiversity and fishery dynamics, making accurate *SST* monitoring essential for the effective management of marine resources (Yang *et al.*, 2021; Zarandi *et al.*, 2024; Kalhoro *et* *al.*, 2025). Furthermore, reliable *SST* observations are instrumental in predicting extreme weather events, thus offering valuable insights into potential climate anomalies (Yang *et al.*, 2021).

In recent years, the integration of *in-situ* and satellite-based *SST* observations has become increasingly prominent. The Copernicus Marine Environment Monitoring Service (CMEMS), in particular, provides extensive and consistent gridded *SST* datasets that support a wide range of oceanographic and climatological studies (Traon *et al.*, 2019). Although *in-situ* measurements, such as buoys and coastal monitoring stations, offer high temporal resolution and accuracy, they are limited in spatial coverage. Conversely, satellite-derived (CMEMS *SST* data) *SST* products can provide wide-area coverage but may suffer from limitations due to atmospheric interference and coarse resolution (Merchant *et al.*, 2014). These discrepancies between data sources underscore the importance of developing standardised methods for comparing and validating *SST* datasets to improve the reliability of climate analyses and marine management systems (Vesnaver *et al.*, 2021; Neo *et al.*, 2023). CMEMS aims to bridge this gap by integrating diverse data sources into high-quality information products tailored for scientific and operational use (Traon *et al.*, 2019).

Advancements in machine learning (ML) algorithms have created significant opportunities to enhance the assessment of *SST* data consistency across different sources (Dell'Aversana, 2023). ML techniques excel at identifying complex, nonlinear relationships within large datasets, patterns that traditional statistical methods may fail to detect (Han *et al.*, 2014; Neo *et al.*, 2023; Erkoç and Doğan, 2024). By leveraging these capabilities, researchers can achieve more accurate intercomparisons between *SST* datasets, improve bias detection, and enhance model reliability for climate and resource management applications (Dell'Aversana, 2021; Shapiro *et al.*, 2023). Furthermore, ML enables the fusion of *in-situ* and satellite data to generate more robust *SST* estimates and forecasts, leading to an improved understanding and prediction of marine and atmospheric processes (Han *et al.*, 2014; Sun *et al.,* 2024).

However, despite the growing use of ML in *SST* modelling, prior studies have rarely addressed the spatial optimisation of *SST* observation networks using ML-driven frameworks. Most existing approaches focus on temporal prediction or bias correction, while the problem of strategically placing new observation points in data-sparse coastal zones remains largely unresolved (Dell'Aversana, 2023). In addition, the concept of virtual *SST* stations, which are statistically inferred observation points that simulate *in-situ* measurements using satellite data and predictive modelling, has not been fully explored in a ML and spatial optimisation context.

The novelty of this study lies in its dual-stage integration of ML and the Analytic Hierarchy Process (AHP): not only validating inter-dataset consistency but also proposing a reproducible and scalable framework for spatially optimised *SST* network expansion. Unlike earlier studies that primarily emphasised temporal prediction, this work demonstrates how ML can be employed as a decision-support tool for network design. Based on 21 *in-situ* stations along the Turkish coasts, CMEMS data are systematically evaluated using multiple ML algorithms, the optimal model is selected via the AHP, and virtual *SST* stations are proposed to address observational gaps.

2. Methods and materials

2.1. Study area and data collection

The spatial domain of this study covers the entire Turkish coastline, encompassing coastal segments of the Mediterranean, Aegean, Marmara, and Black seas. This region is of strategic climatological and oceanographic importance due to its highly dynamic *SST* variability and interaction with regional atmospheric systems. The locations of all stations used in this study are shown in Fig. 1.

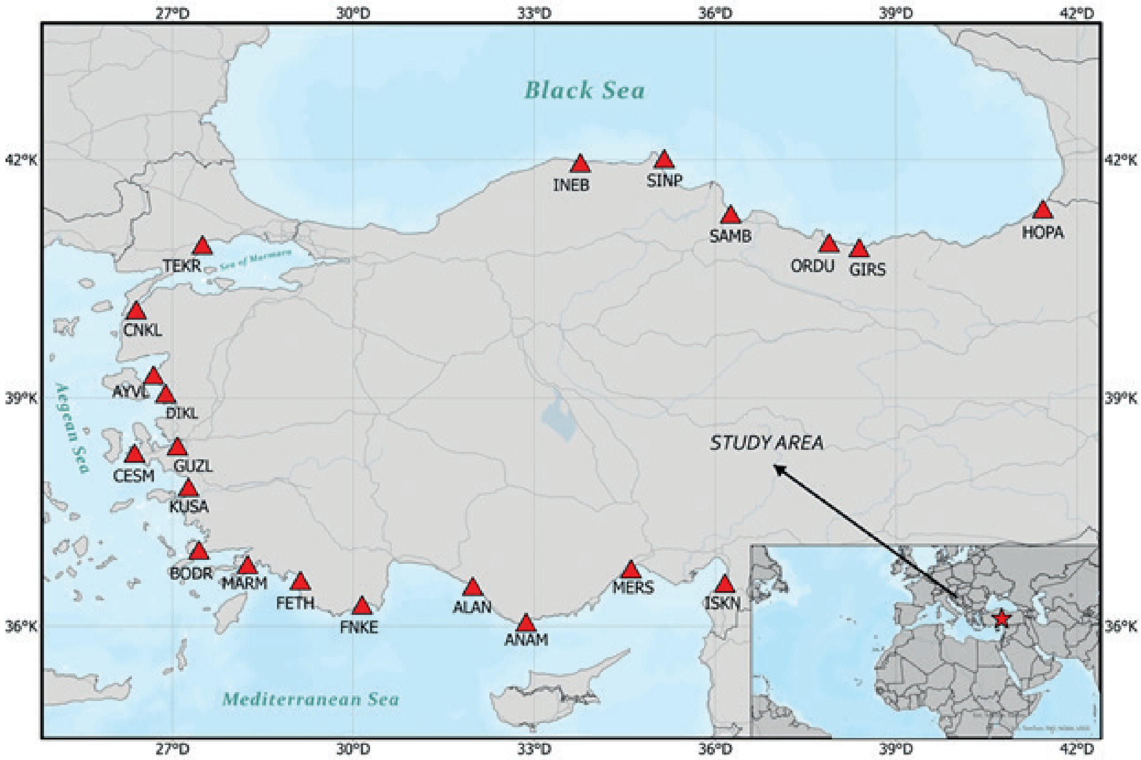

Fig. 1 - The study area.

This analysis employs a 30-year time series (1993–2024) of monthly *SST* data, integrating both *in-situ* measurements and CMEMS *SST* data. *In-situ* data were obtained from 21 coastal meteorological stations operated by the Turkish State Meteorological Service (MGM). These specific stations were selected because they provided continuous records for the entire 30-year period, ensuring temporal consistency and supporting robust long-term trend analysis and model validation. Satellite *SST* data were sourced from the CMEMS. Among the available gridded products, the 1/4° GLOBAL_MULTIYEAR_PHY_ENS_001_031 dataset was selected, as it is widely recognised as the reference product for climate-scale analysis, having undergone extensive validation and frequent use in long-term oceanographic research. Although a higher-resolution (1/24°) product is also available, it is primarily designed for short-term operational forecasting and has been documented to exhibit higher uncertainties in complex coastal and estuarine areas. The selected 1/4° product, in contrast, has been validated and consolidated for long-term applications (Bourdallé-Badie *et al.*, 2023). Both datasets were temporally aligned for the 1993–2024 period. Table 1 provides a summary of the station names, abbreviations, data coverage periods, and the proportion of missing values for both datasets.

Table 1 - Description of the *SST* datasets and station-level information.

Station	Abbreviation	Time Span	MGM data	CMEMS *SST* data
			Gaps (%)	
ALANYA	ALAN	1993-2024	1.3	0.0
ANAMUR	ANAM	1993-2024	0.5	0.0
AYVALIK	AYVL	1993-2024	0.5	0.0
BODRUM	BODR	1993-2024	0.5	0.0
ÇANAKKALE	CNKL	1993-2024	1.6	0.0
ÇEŞME	CESM	1993-2024	3.4	0.0
DİKİLİ	DIKL	1993-2024	0.5	0.0
FETHİYE	FETH	1993-2024	0.5	0.0
FİNİKE	FNKE	1993-2024	0.5	0.0
GİRESUN	GIRS	1993-2024	0.8	0.0
HOPA	HOPA	1993-2024	1.3	0.0
İNEBOLU	INEB	1993-2024	0.8	0.0
İSKENDERUN	ISKN	1993-2024	1.8	0.0
İZMİR BÖLGE	GUZL	1993-2024	0.8	0.0
KUŞADASI	KUSA	1993-2024	0.3	0.0
MARMARİS	MARM	1993-2024	0.8	0.0
MERSİN	MERS	1993-2024	0.8	0.0
ORDU	ORDU	1993-2024	1.1	0.0
SAMSUN BÖLGE	SAMB	1993-2024	0.8	0.0
SİNOP	SINP	1993-2024	0.8	0.0
TEKİRDAĞ	TEKR	1993-2024	0.3	0.0

2.2. Data preparation and modelling approach

Missing values within the *SST* time series were addressed through linear interpolation, a commonly utilised method for resolving short-term temporal gaps in climatological and oceanographic data (Wilks, 2011). All features were subsequently normalised using min-max scaling to ensure comparability across variables and to facilitate model convergence during training (Han *et al.*, 2012). The dataset was, then, partitioned into training (80%) and testing (20%) subsets using stratified random sampling to preserve the temporal distribution of the data.

The modelling framework was constructed to evaluate the predictive capacity of CMEMS-derived *SST* values for estimating *in-situ SST* observations. To this end, the task was framed as a supervised regression problem, in which CMEMS *SST* served as the independent variable, and *in-situ SST* represented the dependent target variable. The functional form of the prediction can be expressed as:

$$Y_t = f(X_t) + \varepsilon_t \tag{1}$$

where X_t denotes the CMEMS *SST* value at time t, Y_t is the estimated *in-situ SST*, and ε_t is the random error term.

Four ML algorithms were employed to model the relationship between CMEMS and *in-situ SST* values: linear regression (LR), support vector regression (SVR), gradient boosting (GB), and artificial neural network (ANN). Each model was trained using identical input features and evaluated under consistent experimental settings to ensure comparability across approaches.

A brief overview of the theoretical assumptions, mathematical formulations, and learning strategies of the employed models is presented in Table 2.

To assess the predictive accuracy and robustness of the models, three widely accepted evaluation metrics were adopted: the root-mean-square error (*RMSE*), mean-absolute error (*MAE*), and coefficient of determination (R^2). These metrics, along with their mathematical formulations and interpretative characteristics, are also included in Table 2. The *RMSE* is particularly sensitive to large errors, the *MAE* captures the average magnitude of all errors regardless of direction, and the R^2 reflects the proportion of variance in the target variable that is explained by the model predictions.

Following the evaluation of individual model performances, the AHP was employed to determine the most appropriate algorithm based on multiple criteria. The AHP allows for structured multi-criteria decision making by quantifying the relative importance of each

Table 2 - Overview of the regression models, their mathematical representations, and performance metrics used in the study.

<table>
<tr><th colspan="3">Model</th><th colspan="3">Formula</th></tr>
<tr><td colspan="3">Linear regression (LR) assumes a linear relationship between the input and the target variable and estimates parameters via ordinary least squares (OLS) (Draper and Smith, 1998).</td><td colspan="3">$SST(t) = \beta_0 + \beta_1 X_t + \varepsilon_t$ (2)
Parameters are estimated using the OLS.</td></tr>
<tr><td colspan="3">Support vector regression (SVR) utilises kernel functions to map data into a high-dimensional space, optimising a cost function that penalises deviations exceeding a predefined ε margin (Smola and Schölkopf, 2004).</td><td colspan="3">Data to a high-dimensional space via kernel functions and solves:
$min_{w,b,\xi,\xi^*} \frac{1}{2}||w||^2 + C\sum \quad (\xi_i + \xi_i^*)]$. (3)
Subject to constraints involving -insensitive loss.</td></tr>
<tr><td colspan="3">Gradient boosting (GB) constructs additive models in a forward stage-wise fashion by optimising residual errors through weak learners (Friedman, 2001).</td><td colspan="3">Constructs learners sequentially:
$F_m(X) = F_{m-1}(X) + \nu h_m(X)$ (4)
where v is the learning rate.</td></tr>
<tr><td colspan="3">Artificial neural network (ANN) learns complex nonlinear mappings through interconnected layers of neurons, where the transformation of inputs is governed by activation functions and learned weights (Goodfellow et al., 2016).</td><td colspan="3">Learns a nonlinear function through layers of neurons:
$\widehat{Y_t} = \sigma(W_2 \cdot \sigma(W_1 X_t + b_1) + b_2)$ (5)
where σ is an activation function and W_1, W_2 are weight matrices.</td></tr>
<tr><td colspan="6">All models (except ANN) underwent hyperparameter tuning via grid search and k-fold cross-validation to optimise performance.</td></tr>
<tr><td colspan="6">Three primary metrics were used to assess model performance:</td></tr>
<tr><td colspan="2">Root-mean-square error (RMSE):</td><td colspan="2">Mean-absolute error (MAE):</td><td colspan="2">Coefficient of determination (R^2):</td></tr>
<tr><td colspan="2">$RMSE = \sqrt{\frac{1}{n}\sum_{i=1}^{n} \quad (Y_i - \widehat{Y_i})^2}$ (6)</td><td colspan="2">$MAE = \frac{1}{n}\sum_{i=1}^{n} \quad |Y_i - \widehat{Y_i}|$ (7)</td><td colspan="2">$R^2 = 1 - \frac{\sum \quad (Y_i - \widehat{Y_i})^2}{\sum \quad (Y_i - \underline{Y})^2}$ (8)</td></tr>
<tr><td colspan="2">Highly sensitive to outliers due to squaring of errors (Willmott and Matsuura, 2005).</td><td colspan="2">Measures the average magnitude of errors regardless of direction (Hyndman and Koehler, 2006).</td><td colspan="2">Indicates of variance explained by the model (Nagelkerke, 1991).</td></tr>
</table>

evaluation metric and computing a final score for each model accordingly (Forman and Gass, 2001; Yüksel, 2012; Jovanović *et al.*, 2013; Torre and Salomon, 2022).

The process involves the steps described as follows.

The AHP framework is used to determine the best-performing algorithm by considering all three evaluation metrics. The process includes:

1. pairwise comparison matrix construction using the Saaty 1–9 scale;
2. normalisation of the matrix and computation of the weight vector;
3. consistency check using the consistency ratio:

$$CI = \frac{\lambda_{max} - n}{n - 1}, \quad CR = \frac{CI}{RI}; \tag{9}$$

4. final score calculation:

$$S_j = \sum_{i=1}^{3} w_i \cdot v_{ij} \tag{10}$$

where v_{ij} is the normalised value of criterion *i* for model *j*. The model with the highest S_j is selected as the most suitable.

This methodology allows the integration of multiple criteria into a single decision framework that is both objective and reproducible.

After selecting the most accurate model, it is used to estimate *SST* values at locations lacking *in-situ* measurements. The model is trained with features such as latitude, longitude, month, and CMEMS *SST*. A station placement constraint of 150 km was introduced between virtual points. This threshold was selected based on typical spatial decorrelation distances for *SST* in semi-enclosed basins such as the Mediterranean and the Black Sea. The constraint also ensures the practical feasibility of integrating these virtual *SST* stations into national-scale monitoring frameworks.

Virtual *SST* station deployment is treated as an optimisation problem, where the objective is to cover spatial gaps with minimal redundancy. The model outputs predictions $\widehat{Y}_{i,t}$ defined by:

$$\widehat{Y_{i,t}} = f(Lat_i, Lon_i, Month_t, CMEMS_{i,t}). \tag{11}$$

The approach enables the targeted expansion of the *SST* observation network, especially in coastal areas with poor coverage, using data-driven logic informed by ML.

2.3. Data analysis

The analysis of *SST* data was carried out to assess the agreement between CMEMS *SST* data and *in-situ* (MGM) observations across 21 coastal stations in Turkey. Initially, classical statistical methods were used to quantify the baseline compatibility between the two datasets. For each station, Pearson correlation coefficients, root-mean-square deviation (*RMSD*), and mean bias values (CMEMS - MGM) were calculated based on temporally matched monthly observations between 1993 and 2024. This provided an initial assessment of the consistency and systematic deviations between the data sources.

Subsequently, a more comprehensive evaluation was conducted using supervised ML techniques to determine the predictive capacity of CMEMS *SST* data with respect to the *in-situ* measurements. Four widely used regression models (i.e. LR, SVR, GB, and ANN) were implemented independently for each of the 21 stations. CMEMS *SST* values were used as inputs and MGM *SST* values as targets. The dataset was divided into training and testing subsets, and model performances were evaluated using *RMSE*, *MAE*, and R^2 metrics.

This dual-phase analysis enabled a robust examination of the agreement between the datasets and allowed for the identification of the most effective model to estimate *in-situ SST* from satellite observations. The modelling results served not only to evaluate dataset consistency, but also to inform the feasibility of generating virtual *SST* stations in areas lacking observational infrastructure.

3. Results

This section presents the outcomes of both statistical and ML-based evaluations of the agreement between CMEMS *SST* data and *in-situ* MGM *SST* datasets for 21 coastal stations in Turkey over the 1993–2024 period. The analysis includes classical statistical comparison metrics as well as regression model performance metrics derived from four ML algorithms.

3.1. Statistical agreement between CMEMS and in-situ SST datasets

The initial assessment of consistency between CMEMS and MGM *SST* datasets was performed using classical statistical metrics, namely the Pearson correlation coefficient and *RMSD*. Results from 21 coastal stations over the 1993–2024 period are summarised in Table 3. In addition, Fig. 2 presents representative *SST* time series together with their mean *RMSD* values for four stations, each selected to represent one of the Turkish seas [FNKE (Mediterranean), BODR (Aegean), TEKR (Marmara), and SINP (Black Sea)]. This approach provides visual examples across different marine regions, while the remaining stations are fully documented in Table 3.

The correlation coefficients between CMEMS and *in-situ* measurements ranged from 0.939 (AYVL) to 0.988 (FNKE), with an average of 0.972. These results indicate a very strong linear relationship across nearly all stations and confirm the robustness of CMEMS *SST* data. *RMSD* values varied between a minimum of 0.8 °C (ALAN, FNKE) and a maximum of 2.8 °C (AYVL), with an overall mean of 1.51 °C.

3.2. Machine learning model performance

To evaluate the capability of CMEMS *SST* data in estimating *in-situ* MGM *SST* data, four supervised regression algorithms, LR, SVR, GB, and ANN, were applied individually for each of the 21 coastal stations. CMEMS *SST* values served as inputs, and MGM *SST* values were used as target outputs. The models were assessed using *RMSE*, *MAE*, and R^2. The full station-by-station results are presented in Table 4.

On average, GB demonstrated the best performance across all stations, achieving a mean *RMSE* of 0.84 °C, *MAE* of 0.66 °C, and R^2 of 0.97. It was followed by SVR and LR, both of which produced comparable outcomes with mean R^2 values of 0.963 and 0.961, respectively. ANN showed the weakest results overall, with R^2 dropping below 0.93 in several stations, especially those in the Black Sea. Spatially, the Mediterranean and Aegean stations exhibited stronger model performance. For example, in stations such as ALAN, FNKE, and MARM, GB consistently

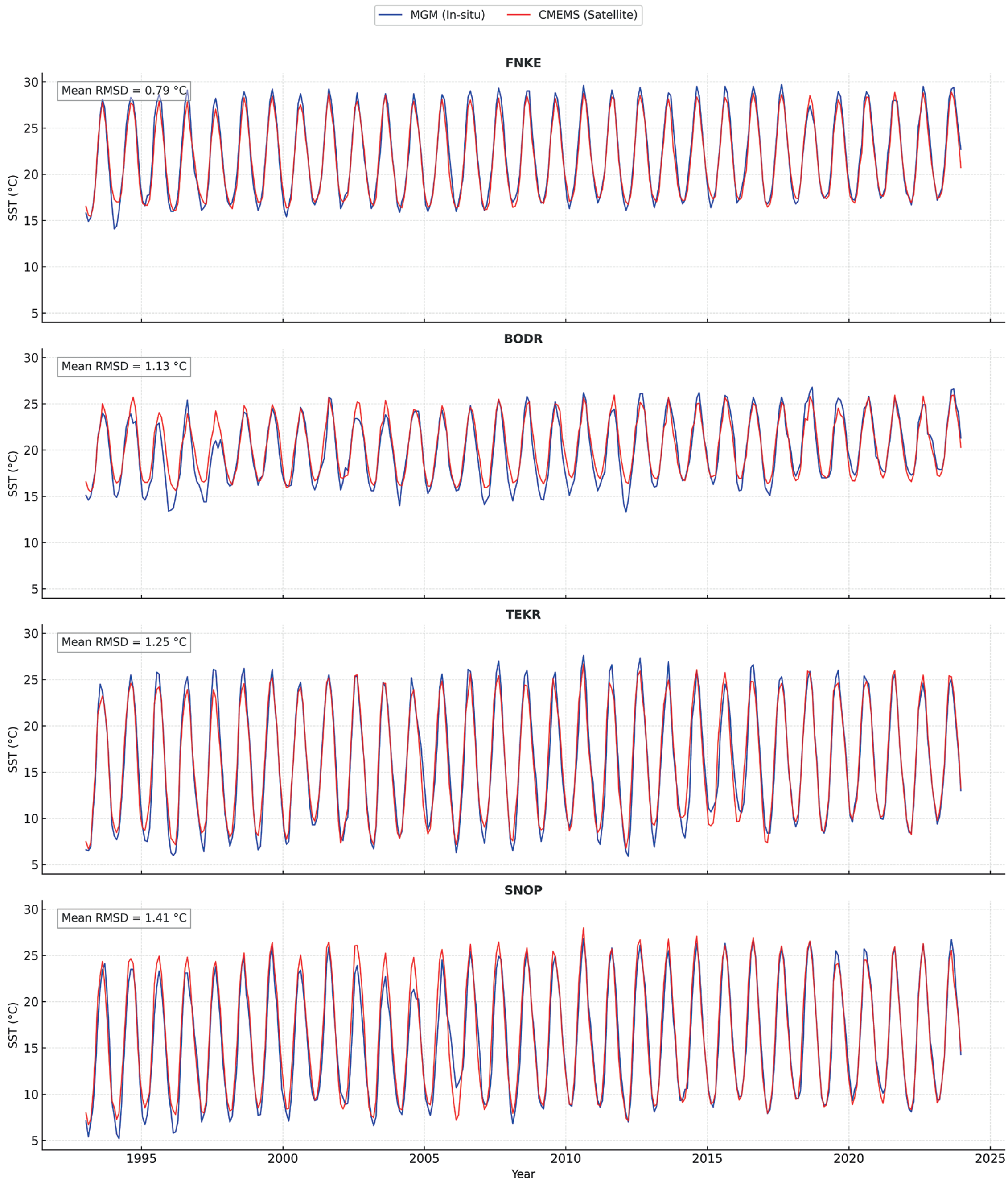

Fig. 2 - Comparison of monthly *SST* time series from MGM *in-situ* observations (blue) and CMEMS satellite products (red) for four representative coastal stations along the Turkish seas: FNKE (Mediterranean), BODR (Aegean), TEKR (Marmara), and SINP (Black Sea) during the 1993–2024 period. The *RMSD* values are indicated in each panel, providing a quantitative measure of agreement between *in-situ* and satellite datasets.

yielded *RMSE* values below 0.60 °C and R^2 above 0.98. In contrast, Black Sea stations like GIRS, and HOPA showed relatively lower performance across all models, with ANN and LR models producing *RMSE* values exceeding 1.5 °C and R^2 values frequently below 0.94. These spatial trends suggest that the stability and thermal structure of southern seas provide a more suitable

Table 3 - Data availability, correlation coefficient, and *RMSD* between CMEMS and MGM *SST* datasets at 21 coastal stations (1993–2024).

MGM station	Data span	Correlation coefficient	*RMSD* (°C)
ALAN	1993-2024	0.99	0.83
ANAM	1993-2024	0.98	0.90
AYVL	1993-2024	0.94	2.84
BODR	1993-2024	0.96	1.13
CNKL	1993-2024	0.98	2.11
CESM	1993-2024	0.96	1.54
DIKL	1993-2024	0.95	1.76
FETH	1993-2024	0.97	1.57
FNKE	1993-2024	0.99	0.79
GIRS	1993-2024	0.97	2.41
HOPA	1993-2024	0.96	2.45
INEB	1993-2024	0.98	1.66
ISKN	1993-2024	0.98	1.11
GUZL	1993-2024	0.98	1.47
KUSA	1993-2024	0.96	1.33
MARM	1993-2024	0.98	0.86
MERS	1993-2024	0.98	1.17
ORDU	1993-2024	0.98	2.35
SAMB	1993-2024	0.98	1.70
SINP	1993-2024	0.98	1.41
TEKR	1993-2024	0.98	1.25

environment for *SST* modelling using satellite data. The relatively high *RMSE* values observed at GIRS and HOPA may be attributed to local environmental factors such as terrestrial runoff, freshwater inflow, and coastal turbidity, which are more pronounced in the north-eastern Black Sea region. These processes may introduce additional *SST* variability that is not well captured by satellite observations, thereby reducing the predictive performance of the models. Similar cross-shelf freshwater and wind-driven processes have also been reported in other narrow shelf systems (Johnson *et al.*, 2024).

Fig. 3 provides illustrative examples of model performance at two representative stations: ALAN in the Mediterranean Sea, where GB achieved the best results (*RMSE* = 0.55 °C, *MAE* = 0.42 °C, and R^2 = 0.98), and HOPA in the Black Sea, where GB also outperformed the other models (*RMSE* = 1.19 °C, *MAE* = 0.95 °C, and R^2 = 0.96). While Fig. 3 highlights these two cases for balance, the full model performance across all stations is comprehensively detailed in Table 4.

These results highlight the robustness of ensemble learning methods, particularly GB, in capturing the complex, nonlinear relationships between CMEMS and MGM *SST* data. Conversely, the relatively lower performance of an ANN model may be attributed to its sensitivity to hyperparameters and susceptibility to overfitting, particularly in coastal zones where *SST* dynamics are more variable. In this study, ANN models were trained using standard architectures and default tuning parameters, which may not have been sufficient to generalise well across all stations. Future implementations could benefit from more rigorous hyperparameter optimisation, dropout regularisation, or early stopping strategies to mitigate overfitting and improve model robustness.

Table 4 - *RMSE*, *MAE*, and R^2 values for LR, SVR, GB, and ANN models applied at each station (1993–2024).

Station	Model	*RMSE*	*MAE*	R^2	Station	Model	*RMSE*	*MAE*	R^2
ALAN	LR	0.78	0.59	0.97	INEB	LR	1.06	0.84	0.96
	SVR	0.79	0.59	0.97		SVR	1.07	0.84	0.96
	GB	0.55	0.43	0.99		GB	0.81	0.64	0.98
	ANN	0.89	0.69	0.96		ANN	1.07	0.84	0.96
ANAM	LR	0.79	0.61	0.96	ISKN	LR	1.00	0.77	0.96
	SVR	0.80	0.61	0.96		SVR	1.02	0.77	0.96
	GB	0.56	0.44	0.98		GB	0.69	0.55	0.98
	ANN	0.89	0.70	0.95		ANN	1.12	0.86	0.95
AYVL	LR	1.91	1.55	0.88	GUZL	LR	1.08	0.84	0.97
	SVR	1.88	1.49	0.88		SVR	1.08	0.85	0.97
	GB	1.36	1.09	0.94		GB	0.81	0.62	0.98
	ANN	1.90	1.54	0.88		ANN	1.36	1.12	0.95
BODR	LR	1.02	0.82	0.91	KUSA	LR	1.03	0.83	0.93
	SVR	1.02	0.82	0.91		SVR	1.01	0.81	0.93
	GB	0.75	0.59	0.95		GB	0.76	0.60	0.96
	ANN	1.10	0.89	0.90		ANN	1.33	1.07	0.88
CNKL	LR	1.25	0.99	0.95	MARM	LR	0.73	0.58	0.96
	SVR	1.22	0.97	0.96		SVR	0.74	0.58	0.96
	GB	0.88	0.68	0.98		GB	0.54	0.42	0.98
	ANN	1.23	0.97	0.96		ANN	0.78	0.62	0.96
CESM	LR	1.37	1.09	0.91	MERS	LR	0.97	0.76	0.96
	SVR	1.37	1.08	0.91		SVR	0.99	0.77	0.96
	GB	1.05	0.83	0.95		GB	0.70	0.56	0.98
	ANN	1.57	1.26	0.89		ANN	1.25	1.02	0.94
DIKL	LR	1.34	1.02	0.91	ORDU	LR	1.28	1.03	0.95
	SVR	1.36	1.03	0.91		SVR	1.29	1.03	0.95
	GB	0.97	0.77	0.95		GB	0.90	0.72	0.98
	ANN	1.34	1.02	0.91		ANN	1.28	1.03	0.95
FETH	LR	1.06	0.85	0.94	SAMB	LR	1.21	0.89	0.96
	SVR	1.07	0.86	0.94		SVR	1.24	0.90	0.96
	GB	0.83	0.65	0.97		GB	0.87	0.64	0.98
	ANN	1.22	0.98	0.92		ANN	1.26	0.94	0.96
FNKE	LR	0.68	0.50	0.98	SINP	LR	1.29	0.99	0.96
	SVR	0.69	0.51	0.98		SVR	1.30	1.00	0.95
	GB	0.49	0.38	0.99		GB	0.96	0.73	0.98
	ANN	0.77	0.58	0.97		ANN	1.29	0.99	0.96
GIRS	LR	1.59	1.20	0.93	TEKR	LR	1.23	0.91	0.96
	SVR	1.65	1.20	0.93		SVR	1.24	0.94	0.96
	GB	1.11	0.85	0.97		GB	0.89	0.68	0.98
	ANN	1.59	1.20	0.93		ANN	1.34	1.05	0.96
HOPA	LR	1.68	1.33	0.93					
	SVR	1.71	1.33	0.92					
	GB	1.20	0.96	0.96					
	ANN	1.72	1.37	0.92					

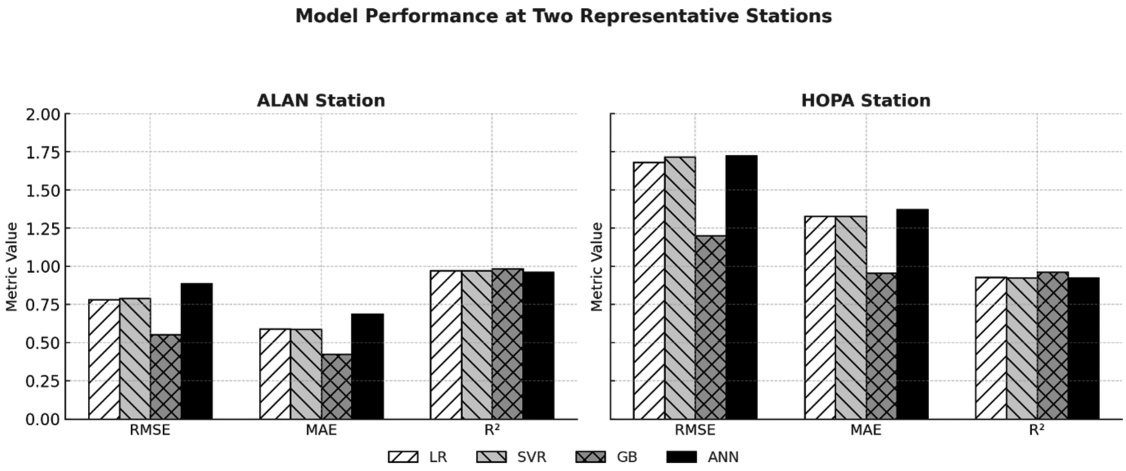

Fig. 3 - Comparative evaluation of four ML models (LR, SVR, GB, and ANN) at two representative coastal stations: a) ALAN (Mediterranean Sea, strong model performance) and b) HOPA (Black Sea, relatively weaker performance). Performance metrics include *RMSE*, *MAE*, and R^2.

3.3. AHP-based model selection

To determine the most suitable ML model for *SST* estimation, the AHP was employed using three evaluation criteria: *RMSE*, *MAE*, and R^2. These criteria were chosen due to their widespread use in regression model evaluation. Equal weighting was adopted based on similar multi-criteria ML evaluations in the literature (e.g. Rady and El-Sheikh, 2021; Zakaria *et al.*, 2022; Susiawati and Kurniawan, 2023), where no domain-specific or expert-informed preference was available. In future applications, expert judgment or domain knowledge could guide a more tailored weighting scheme.

Each model's performance was normalised across all three criteria. For *RMSE* and *MAE* (where lower values are better) criteria, inverse normalisation was applied, while for R^2 (where higher values are better), direct normalisation was used. Table 5 presents the computed AHP scores.

The results clearly indicate that GB is the top-performing model, achieving the highest AHP score of 1.26, followed by SVR (1.15) and LR (1.13). The ANN ranked last with a score of 0.99, primarily due to its relatively higher error values and lower R^2. These findings are consistent with the individual model performance analysis in Section 3.2.

The superiority of GB in the AHP framework highlights its robustness, high predictive accuracy, and ability to generalise across diverse spatial and temporal conditions. Therefore, GB was selected as the optimal model for further evaluation and potential virtual *SST* station estimation presented in the next section.

Table 5 - AHP-based ranking of ML models based on average *RMSE*, *MAE*, and R^2 values across all stations.

Model	*RMSE*	*MAE*	R^2	AHP Score
LR	1.02	0.79	0.96	1.13
SVR	1.01	0.77	0.96	1.15
GB	0.84	0.66	0.97	1.26
ANN	1.24	0.94	0.95	0.99

3.4. Virtual SST station potential

To improve the spatial resolution of *SST* observations along the Turkish coastline, a ML-based spatial gap analysis was conducted to propose virtual *SST* station locations. The aim was to identify coastal regions that are not covered by existing *in-situ* MGM stations yet exhibit high predictive capacity based on CMEMS *SST* data.

This analysis utilised the GB algorithm, which was identified as the most effective regression model through comparative evaluation using the AHP, considering performance metrics such as *RMSE*, *MAE*, and R^2. Across 21 operational MGM coastal stations, the GB model demonstrated high predictive power, with an average R^2 of 0.97, *RMSE* of 0.84 °C, and *MAE* of 0.66 °C, using CMEMS satellite *SST* values as inputs and MGM *SST* records as targets.

After training and validation, spatial segments along the Turkish coastline were analysed for observational gaps exceeding 150 km, based on the current distribution of MGM stations. These segments were further filtered based on GB model performance in neighbouring regions. Only the segments satisfying the following criteria were considered for virtual *SST* station placement:

- high model reliability in surrounding stations (R^2 > 0.97 and *RMSE* < 1.0 °C);
- temporal continuity and stability of CMEMS *SST* data;
- geographic feasibility in terms of shoreline access;
- absence of nearby redundant observation nodes;
- potential for integration into national *SST* monitoring frameworks.

As a result, eight virtual *SST* station locations were proposed to fill observational gaps, particularly in underrepresented regions of the Black Sea, Marmara, Aegean, and Mediterranean coasts. The average spacing between proposed virtual *SST* stations was approximately 170 km, with the maximum identified gap exceeding 450 km. These locations are presented in Fig. 4, where yellow triangles represent the virtual *SST* station proposals, and red triangles indicate the existing MGM *SST* network.

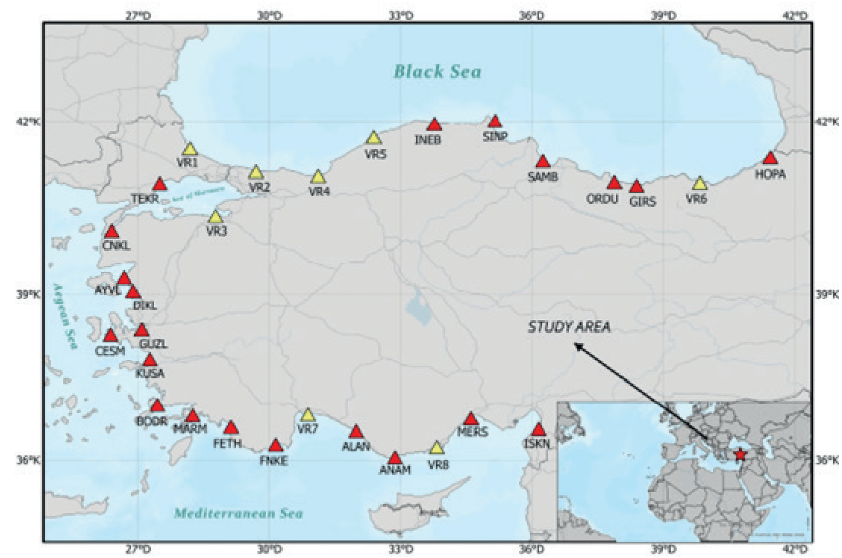

Fig. 4 - Distribution of *in-situ* MGM coastal *SST* stations (red triangles) and proposed virtual *SST* stations (yellow triangles; VR1–VR8) along the Turkish coasts of the Black Sea, Marmara Sea, Aegean Sea, and Mediterranean Sea. Station abbreviations are as indicated in Table 1 and details of the virtual *SST* stations are provided in Table 6. The inset shows the study area in a global context.

By leveraging the generalisability of the ML model and a quantitative spatial coverage analysis, the proposed virtual *SST* stations are both statistically justified and geographically strategic. This approach introduces a reproducible and scalable framework for enhancing national *SST* monitoring capabilities, particularly in complex, semi-enclosed sea regions such as those surrounding Turkey.

In addition to the spatial placement of virtual *SST* stations, their validity was tested by comparing the CMEMS-derived *SST* values at virtual *SST* station locations with the average *SST* of the two geographically nearest *in-situ* MGM and CMEMS stations. The results revealed that the differences between virtual *SST* station values and reference station averages remained mostly within ±1 °C (except for VR1 and VR6), reinforcing the reliability and realism of the proposed virtual *SST* stations. These values are consistent with acceptable *RMSD* thresholds cited in the *SST* validation literature (Reynolds *et al.*, 2007). Table 6 summarises the CMEMS *SST* predictions at virtual *SST* stations, their reference station pairs, and the deviations from reference averages. These results indicate that the virtual *SST* stations can be treated analogously to real *in-situ* observations for both climatological assessments and operational monitoring.

Table 6 - CMEMS-based *SST* predictions at virtual *SST* stations and comparison with reference station averages (*SST* values are long-term averages derived from CMEMS: 1993–2024).

Virtual *SST* station	Reference stations	*SST* (CMEMS-based °C)	MGM Avg (°C)	CMEMS Avg (°C)	DiffVR-MGM (°C)	DiffVR-CMEMS (°C)
VR1	INEB + SINP	16.81	15.16	15.99	0.83	1.66
VR2	INEB + SINP	16.48	15.16	15.99	0.49	1.32
VR3	TEKR + CNKL	17.2	16.35	16.96	0.23	0.85
VR4	INEB + SINP	16.43	15.16	15.99	0.45	1.28
VR5	INEB + SINP	15.87	15.16	15.99	–0.11	0.71
VR6	GIRS + HOPA	18.00	16.14	17.86	0.14	1.86
VR7	ALAN + FNKE	22.21	22.16	22.03	0.17	0.05
VR8	ANAM + MERS	22.36	22.02	22.24	0.12	0.34

4. Discussion

This study contributes to the expanding literature on *SST* monitoring and the integration of *in-situ* and satellite data by demonstrating the viability of ML techniques for assessing and enhancing data consistency. Previous studies, such as Pisano *et al.* (2020) and Yang *et al.* (2021), have emphasised the critical role of *SST* in regulating atmospheric dynamics and forecasting extreme weather events. In this context, ensuring the reliability and spatial continuity of *SST* observations is paramount for both climate science and operational forecasting.

4.1. Dataset agreement and regional variability

The results of classical *RMSD* and correlation analyses confirmed that CMEMS satellite *SST* data are broadly consistent with MGM *in-situ* measurements across most of the Turkish coastline. However, regional differences provide important insights into the strengths and limitations of CMEMS *SST* products. In the north-eastern Black Sea, *RMSD* values exceeding 2 °C reflect the influence of freshwater inflows, turbidity, and strong terrestrial runoff, which are not fully captured in CMEMS datasets. Similar challenges have been documented in other narrow-shelf seas, where satellite retrievals are sensitive to high sediment loads and variable atmospheric conditions (Merchant *et al.*, 2014). Although *RMSD* values above 2 °C may appear locally, they remain within the upper bounds of acceptable thresholds reported in previous *SST* comparison studies (Jiménez-Muñoz *et al.*, 2014), underscoring that such deviations are not uncommon in complex coastal environments. In contrast, the Aegean and Mediterranean coasts exhibited relatively low *RMSD* values, consistent with their stable thermal stratification and reduced land-sea interactions. The Marmara Sea presented an intermediate case, reflecting its semi-enclosed nature and exchange dynamics with both the Black Sea and Aegean. These spatial patterns highlight the necessity to consider regional oceanographic and atmospheric processes when evaluating *SST* dataset consistency.

4.2. Model performance

The integration of ML methods revealed clear differences in model performance. GB consistently outperformed other models, achieving R^2 values above 0.97 and *RMSE* values below 1.1 °C across most stations. This superior performance can be attributed to the ensemble nature of GB, which effectively captures complex nonlinear relationships by iteratively correcting residual errors (Friedman, 2001). By comparison, the ANNs exhibited weaker results in several Black Sea stations, likely due to their sensitivity to hyperparameter choices and susceptibility to overfitting in regions with high variability. LR and SVR performed reasonably well but failed to capture localised anomalies. These findings align with previous research (Han *et al.*, 2014; Neo *et al.*, 2023) demonstrating the advantage of ensemble learning approaches for environmental datasets. Importantly, the use of the AHP added a structured decision-making framework, ensuring that multiple performance metrics were objectively balanced and that GB was not selected solely on statistical grounds but through a transparent multi-criteria evaluation.

4.3. Virtual SST stations as a novel contribution

One of the most innovative outcomes of this study is the introduction of virtual *SST* stations. By combining ML model performance with geospatial analysis, eight strategically located virtual *SST* stations were proposed to fill gaps exceeding 150 km along the Turkish coasts. Unlike conventional approaches that often rely on interpolation or heuristic placement rules, this framework leverages data-driven decision logic, ensuring that proposed stations are both statistically justified and geographically feasible. The small differences between virtual *SST* station-derived *SST* estimates and neighbouring *in-situ* observations (mostly within ±1 °C) reinforce the reliability of this approach. This result positions virtual *SST* stations not as a theoretical exercise but as a practical tool that could be directly integrated into national *SST* monitoring frameworks. Such integration could significantly improve spatial coverage and reduce uncertainties in regional *SST* analyses, particularly in semi-enclosed seas where observational gaps are most pronounced.

4.4. Broader scientific and socio-economic implications

Beyond methodological innovation, the proposed framework holds practical significance for climate and resource management. The improved spatial resolution of *SST* data can support climate change assessments by identifying regional warming patterns and marine heatwave events, which are increasing in frequency and intensity in semi-enclosed seas. Furthermore, enhanced *SST* monitoring directly benefits fishery management, as shifts in temperature regimes are closely tied to fish distribution and spawning behaviour (Kalhoro *et al.*, 2025). From a policy perspective, integrating virtual *SST* stations into national networks would contribute to global initiatives such as the Copernicus Climate Change Service (C3S) and the Global Ocean Observing System (GOOS), thereby aligning local efforts with international monitoring priorities. By positioning ML as both a scientific and operational tool, this study demonstrates its capacity to bridge gaps between academic research and applied marine management.

4.5. Limitations

Despite these promising outcomes, several limitations should be acknowledged. First, the CMEMS dataset used in this study had a spatial resolution of 1/4°, which is the extensively validated reference product for climate-scale analyses. While a higher-resolution (1/24°) product also exists, it is primarily optimised for short-term operational forecasting and carries higher uncertainties in coastal and estuarine environments, as reported in CMEMS quality information documents. For this reason, the 1/4° product was chosen here; however, future research could explore the added value of the 1/24° dataset for reducing coastal uncertainties. Nevertheless, the general constraint of CMEMS products in nearshore and estuarine waters remains a critical limitation, as fine-scale processes may not be adequately resolved.

Second, this study was limited to surface *SST*, even though CMEMS provides three-dimensional outputs. Incorporating depth-dependent diagnostics could provide a more comprehensive understanding of subsurface processes that strongly influence surface dynamics in stratified basins such as the Black Sea. In addition, CMEMS *SST* data can be significantly affected by seasonal cloud cover, which reduces data availability and may bias long-term statistics during certain months.

Third, while monthly averages were chosen for temporal consistency, daily data could capture short-term variability and extreme events that may be masked in aggregated datasets. Moreover, the present analysis only considered CMEMS *SST* as the main predictor. The inclusion of other covariates such as river discharge, turbidity, or wind forcing could improve the robustness of predictive models in future work.

From an operational perspective, the virtual *SST* station framework, although statistically robust, has not yet been independently validated with field campaigns. Future studies should therefore combine satellite-driven virtual *SST* station estimates with targeted *in-situ* measurements to confirm their operational reliability. Such independent validation will be essential to demonstrate the practical feasibility of virtual *SST* stations within national and international monitoring frameworks.

5. Conclusions

This study presents an integrated methodology for evaluating and enhancing coastal *SST* monitoring networks through ML and spatial analysis. Across 21 MGM coastal stations, the GB model achieved R^2 = 0.97, *RMSE* = 0.84 °C, and *MAE* = 0.66 °C, validating the use of CMEMS data for generating *SST* estimates at locations lacking direct observations.

Based on these findings, eight virtual *SST* stations were proposed in spatial gaps exceeding 150 km between operational stations. These stations were strategically selected in the Black Sea, Marmara, Aegean, and Mediterranean regions, taking into account model performance, data continuity, and coastal accessibility.

The novelty of this work lies in its dual-stage framework: i) integrating ML with the AHP for robust model selection, and ii) applying the virtual *SST* station concept for the first time to optimise monitoring network design along the Turkish coasts. Unlike previous studies that mainly focused on temporal prediction or bias correction, our approach provides a reproducible and scalable methodology for spatial optimisation of *SST* observation networks.

This framework not only contributes to the advancement of *SST* monitoring methodologies but also offers direct relevance for operational climate services and marine resource management. Beyond Turkey, the framework is well aligned with global and regional initiatives such as the C3S and GOOS, which emphasise integrated and cost-effective coastal monitoring. It can support climate change impact assessments, operational forecasting, and sustainable marine resource management. At a broader scale, it can serve as a model for similar efforts in other coastal and semi-enclosed sea regions, providing an efficient, scalable, and scientifically robust solution for addressing spatial gaps in environmental monitoring systems.

Acknowledgments. The author extends gratitude to all data providers. *In-situ* sea surface temperature (*SST*) data used in this study were obtained from the Turkish State Meteorological Service (MGM) and are available through the relevant sales offices of the institution upon request. Gridded *SST* data were acquired from the Copernicus Marine Environment Monitoring Service (CMEMS) and can be freely downloaded from their official website: https://marine.copernicus.eu/ (accessed March 2025, data catalogue: GLOBAL_MULTIYEAR_PHY_ENS_001_031). Researchers interested in the data or methodology used in this study may contact the corresponding author via email. ChatGPT was utilised for English translations and checks in the text.

REFERENCES

Bell R.G. and Goring D.G.; 1998: *Seasonal variability of sea level and sea-surface temperature on the north-east coast of New Zealand.* Estuarine Coastal Shelf Sci., 46, 307-318, doi: 10.1006/ecss.1997.0286.

Bourdallé-Badie R., Karioua S., Carabin F., Cipollone A., Zuo H., Parent L., Storto A., Wang C., Garric G., Régnier C. and Drévillon M.; 2024: *Quality Information Document (QUID) for the Global Ocean Reanalysis Multi-Model Ensemble Product (GLOBAL_MULTIYEAR_PHY_ENS_001_031, Issue 1.3, June 2024).* Copernicus Marine Environment Monitoring Service (CMEMS), 39 pp., available at: https://catalogue.marine.copernicus.eu/documents/QUID/CMEMS-GLO-QUID-001-031.pdf

Chapanov Y., Ron C. and Vondrák J.; 2017: *Decadal cycles of Earth rotation, mean sea level and climate, excited by solar activity.* Acta Geodyn. Geomater., 14, 241-250, doi: 10.13168/AGG.2017.0007.

Dell'Aversana P.; 2021: *Deep learning for automatic classification of mineralogical thin sections*. Bull. Geoph. Ocean., 62, 455-466, doi: 10.4430/bgo00367.

Dell'Aversana P.; 2023: *Inversion of geophysical data supported by reinforcement learning.* Bull. Geoph. Ocean., 64, 45-60, doi: 10.4430/bgo00411.

Draper N.R. and Smith H.; 1998: *Applied regression analysis*, *3rd ed.* Wiley, New York, NY, USA, 735 pp.

Erkoç M.H. and Doğan U.; 2024: *Machine learning models applied to altimetry era tide gauge and grid altimetry data for comparative long-term trend estimation: a study from Shikoku Island, Japan.* Appl. Ocean Res., 150, 104132, doi: 10.1016/j.apor.2024.104132.

Forman E. and Gass S.; 2001: *The analytic hierarchy process—an exposition.* Oper. Res., 49, 469-486, doi: 10.1287/opre.49.4.469.11231.

Friedland K.D. and Hare J.A.; 2007: *Long-term trends and regime shifts in sea surface temperature on the continental shelf of the northeast United States.* Cont. Shelf Res., 27, 2313-2328, doi: 10.1016/j.csr.2007.06.001.

Friedman J.H.; 2001: *Greedy function approximation: a gradient boosting machine.* Ann. Stat., 29, 1189-1232, doi: 10.1214/aos/1013203451.

Goodfellow I., Bengio Y. and Courville A.; 2016: *Deep learning*. MIT Press, Cambridge, MA, USA, 800 pp.

Han J., Kamber M. and Pei J.; 2012: *Data mining trends and research frontiers.* In: Data mining 3rd ed., The Morgan Kaufmann Series in Data Management Systems. pp. 585-631, doi: 10.1016/B978-0-12-381479-1.00013-7.

Han X., Franssen H., Montzka C. and Vereecken H.; 2014: *Soil moisture and soil properties estimation in the community land model with synthetic brightness temperature observations.* Water Resour. Res., 50, 6081-6105, doi: 10.1002/2013wr014586.

Hyndman R.J. and Koehler A.B.; 2006: *Another look at measures of forecast accuracy.* Int. J. Forecasting, 22, 679-688, doi: 10.1016/j.ijforecast.2006.03.001.

Jiménez-Muñoz J.C., Sobrino J.A., Skokovic D., Mattar C. and Cristóbal J.; 2014: *Land surface temperature retrieval methods from Landsat-8 thermal infrared sensor data.* IEEE Geosci. Remote Sens. Lett., 11, 1840–1843. https://doi.org/10.1109/LGRS.2014.2312032.

Johnson E.E., Collins C., Suanda S.H., Wing S.R., Currie K.I., Vance J., Smith R.O.; 2024: *Drivers of neritic water intrusions at the subtropical front along a narrow shelf*. Cont. Shelf Res., 277, 105248. doi: 10.1016/j.csr.2024.105248.

Jovanović J., Krivokapić Z. and Vujović A.; 2013: *Evaluation of environmental impacts using backpropagation neural network.* Kybernetes, 42, 698-710, doi:10.1108/k-03-2013-0055.

Kalhoro M.A., Ye H., Liu C., Zhu L., Liang Z. and Tang D.; 2025: *Impact of sea surface temperature fronts on the spatial distribution of jellyfish in the northern Arabian Sea.* Estuarine Coastal Shelf Sci., 312, 109033, doi: 10.1016/j.ecss.2024.109033.

Merchant C., Embury O., Roberts-Jones J., Fiedler E., Bulgin C., Corlett G. and Donlon C.; 2014: *Sea surface temperature datasets for climate applications from phase 1 of the European Space Agency Climate Change Initiative (SST CCI).* Geosci. Data J., 1, 179-191, doi: 10.1002/gdj3.20.

Nagelkerke N.J.D.; 1991: *A note on a general definition of the coefficient of determination*. Biometrika, 78, 691-692, doi: 10.1093/biomet/78.3.691.

Neo V., Zinke J., Fung T., Merchant C., Zawada K., Krawczyk H. and Maina J.; 2023: *Inconsistent coral bleaching risk indicators between temperature data sources.* Earth Space Sci., 10, doi: 10.1029/2022ea002688.

Pisano A., Marullo S., Artale V., Falcini F., Yang C., Leonelli F. and Nardelli B.; 2020: *New evidence of Mediterranean climate change and variability from sea surface temperature observations.* Remote Sens., 12, 132, doi: 10.3390/rs12010132.

Rady E. and El-Sheikh A.; 2021: *The distribution of the coefficient of determination in linear regression model: a review.* J. Univ. Shanghai Sci. Tech., 23, 126-127, doi: 10.51201/jusst/21/08481.

Reynolds R.W., Smith T.M., Liu C., Chelton D.B., Casey K.S. and Schlax M.G.; 2007: *Daily high-resolution blended analyses for sea surface temperature*. J. Clim., 20(22), 5473–5496, doi: 10.1175/2007JCLI1824.1.

Shapiro G., González-Ondina J., Salim M. and Tu J.; 2023: *A comparison of stochastic and deterministic downscaling in eddy resolving ocean modelling: the Lakshadweep Sea case study.* J. Mar. Eng., 11, 363, doi: 10.3390/jmse11020363.

Smola A.J. and Schölkopf B.; 2004: *A tutorial on support vector regression.* Statistics Comput., 14, 199-222, doi: 10.1023/B:STCO.0000035301.49549.88.

Sun X., Lu T. and Wang Z.; 2024: *Comparative analysis of different deep learning algorithms for the prediction of marine environmental parameters based on CMEMS products.* Acta Geodyn. Geomater., 21, 343-363, doi: 10.13168/AGG.2024.0028.

Susiawati S. and Kurniawan B.; 2023: *Goodness test of adaptability to model of technical changes and test of forecasting accuracy.* J. Statistics Data Sci., 2, 22-28, doi: 10.33369/jsds.v2i1.27257.

Torre N.M.M. and Salomon V.A.P.; 2022: *Multi-criteria assessment of spare parts of hydraulic systems.* In: Proc. The International Symposium on the Analytic Hierarchy Process (ISAH), Web Conference, doi: 10.13033/isahp.y2022.050.

Traon P.Y., Reppucci A., Alvarez Fanjul E., Aouf L., Behrens A., Belmonte M., Bentamy A., Bertino L., Brando V.E, Kreiner M., Benkiran M., Carval T., Ciliberti S.A., Claustre H., Clementi E., Coppini G., Cossarini G., De Alfonso M., Delamarche A., Dibarboure G., Dinessen F., Drevillon M., Drillet Y., Faugere Y., Fernández V., Fleming A., Garcia-Hermosa M.I., Sotillo M.G., Garric G., Gasparin F., Giordan C., Gehlen M., Gregoire M.L., Guinehut S., Hamon M., Harris C., Hernandez F., Hinkler J.B., Hoyer J., Karvonen J., Kay S., King R., Lavergne T., Lemieux-Dudon B., Lima L., Mao C., Martin M.J., Masina S., Melet A., Buongiorno Nardelli B., Nolan G., Pascual A., Pistoia J., Palazov A., Piolle J.F., Pujol M.I., Pequignet A.C., Peneva E., Pérez Gómez B., Petit de la Villeon L., Pinardi N., Pisano A., Pouliquen S., Reid R., Remy E., Santoleri R., Siddorn J., She J., Staneva J., Stoffelen A., Tonani M., Vandenbulcke L., von Schuckmann K., Volpe G., Wettre C. and Zacharioudaki A.; 2019: *From observation to information and users: the Copernicus Marine Service perspective.* Front. Mar. Sci., 6, 234, doi: 10.3389/fmars.2019.00234.

Vesnaver A., Busetti M. and Baradello L.; 2021: *Chirp data processing for fluid flow detection at the Gulf of Trieste (northern Adriatic Sea).* Bull. Geophys. Ocean., 62, 365-386, doi: 10.4430/bgo00361.

Wilks D.S.; 2011: *Statistical methods in the atmospheric sciences, 3rd ed.* International Geophysics Series, Academic Press, Oxford, UK, Vol. 100.

Willmott C.J. and Matsuura K.; 2005: *Advantages of the mean absolute error (MAE) over the root mean square error (RMSE) in assessing average model performance.* Clim. Res., 30, 79-82, doi: 10.3354/cr030079.

Yang C., Leonelli F., Marullo S., Artale V., Beggs H., Nardelli B. and Pisano A.; 2021: *Sea surface temperature intercomparison in the framework of the Copernicus Climate Change Service (C3S).* J. Clim., 34, 5257-5283, doi: 10.1175/jcli-d-20-0793.1.

Yüksel M.; 2012: *Evaluating the effectiveness of the chemistry education by using the analytic hierarchy process.* Int. Educ. Stud., 5, 79-91, doi: 10.5539/ies.v5n5p79.

Zakaria A., Gordor B. and Nkansah B.; 2022: *On the coefficient of determination ratio for detecting influential outliers in linear regression analysis.* Am. J. Theor. Appl. Stat., 11, 27-35, doi: 10.11648/j.ajtas.20221101.14.

Zarandi M.Z., Barzandeh A., Hassanzadeh S. and Zoljoodi Zarandi R.; 2024: *Investigating an upwelling system along the eastern Makran coast.* Bull. Geoph. Ocean., 65, 123-138, doi: 10.4430/bgo00441.

Corresponding author: Muharrem Hilmi Erkoç
Department of Geomatic Engineering, Yildiz Technical University,
Davutpasa Cad. No.1, 34220, Esenler-İstanbul, Turkey
Phone: +902123835288; e-mail: mherkoc@yildiz.edu.tr